Variation of the magnetic ordering in GdT_2Zn_{20} (T= Fe, Ru, Os, Co, Rh and Ir) and its correlation with the electronic structure of isostructural YT_2Zn_{20}

Shuang Jia[1,2], Ni Ni[1,2], G. D. Samolyuk[1], A. Safa-Sefat[1], K. Dennis[1],
Hyunjin Ko[1,3], G. J. Miller[1,3], S. L. Bud'ko[1,2], P. C. Canfield[1,2]

[1]*Ames Laboratory, USDOE*

[2]*Department of Physics and Astronomy*

[3]*Department of Chemistry,*

Iowa State University

Ames, Iowa 50011, USA

Abstract

Magnetization, resistivity and specific heat measurements were performed on the solution-grown, single crystals of six GdT_2Zn_{20} (T = Fe, Ru, Os, Co, Rh and Ir) compounds, as well as their Y analogues. For the Gd compounds, the Fe column members manifest a ferromagnetic (FM) ground state (with an enhanced Curie temperature, T_C, for T = Fe and Ru), whereas the Co column members manifest an antiferromagnetic (AFM) ground state. Thermodynamic measurements on the YT_2Zn_{20} revealed that the enhanced T_C for $GdFe_2Zn_{20}$ and $GdRu_2Zn_{20}$ can be understood within the framework of Heisenberg moments embedded in a nearly ferromagnetic Fermi liquid. Furthermore, electronic structure calculations indicate that this significant enhancement is due to large, close to the Stoner FM criterion, transition metal partial density of states at Fermi level, whereas the change of FM to AFM ordering is associated with filling of electronic states with two additional electrons per formula unit. The degree of this sensitivity is addressed by the studies of the pseudo-ternary compounds $Gd(Fe_xCo_{1-x})_2Zn_{20}$ and $Y(Fe_xCo_{1-x})_2Zn_{20}$ which clearly reveal the effect of $3d$ band filling on their magnetic properties.

PACS numbers: 75.50.Cc, 75.50.Ee, 75.30.Cr, 71.20.Lp

I. INTRODUCTION

Magnetism of rare earth intermetallics, determined by the interaction between $4f$ local moments and conduction electrons, especially the d-band conduction electrons of transition metals, has been of interest to physicists for several decades.[1, 2] Recently, studies of the dilute, rare earth bearing, intermetallic compounds, RT_2Zn_{20} (R = rare earth, T = transition metal in Fe, Co or neighboring groups), revealed varied, exotic magnetic properties.[3, 4, 5] Containing less than 5 at. % rare earth ions which, although dilute, fully occupy a unique crystallographic site, these compounds allow for the study of local and hybridizing moment magnetism in a regime that approaches the single ion limit while preserving periodicity. Previous studies of these compounds have indicated that they can serve as model systems for a variety of physical phenomenon ranging from a nearly ferromagnetic Fermi liquid (NFFL) (YFe_2Zn_{20} and $LuFe_2Zn_{20}$),[3] to greatly enhanced ferromagnetic (FM) order in $GdFe_2Zn_{20}$,[3, 5] all the way to heavy fermion ground states in YbT_2Zn_{20} (T = Fe, Ru, Os, Co, Rh and Ir).[4]

The RT_2Zn_{20} series of compounds were discovered in 1997 by Nasch et al.[6] These compounds assume the isostructural, cubic, $CeCr_2Al_{20}$ structure[7, 8, 9], in which the R and T ions each occupy their own single, unique crystallographic site with cubic and trigonal point symmetry respectively, and the Zn ions have three unique crystallographic sites (Fig. 1). The coordination polyhedra for R and T are fully comprised of Zn, meaning that there are no R-R, T-T or R-T nearest neighbors and the shortest R-R spacing is $\sim$ 6 Å. The nearest-neighbor and next-nearest-neighbor shells of the R are all Zn, forming an all Zn Frank-Kasper polyhedron around, and isolating the site.[6] RT_2Zn_{20} compounds had been found to form for T = Fe, Ru, Co and Rh, but no thermodynamic or transport property measurements were reported. As part of this study we have extended the range of known RT_2Zn_{20} compounds to T = Os and Ir series.

In rare earth containing series of intermetallic compounds, R = Gd members give the clearest indication of the strength and sign of the magnetic interaction, without any complications associated with crystalline electric field splitting of the Hund's rule ground state multiplet. In order to better understand the RT_2Zn_{20} series of compounds, in this paper we examine the thermodynamic and transport properties of six GdT_2Zn_{20} (T = Fe, Ru, Os, Co, Rh and Ir) compounds as well as their R = Y analogues. We found FM transitions in the

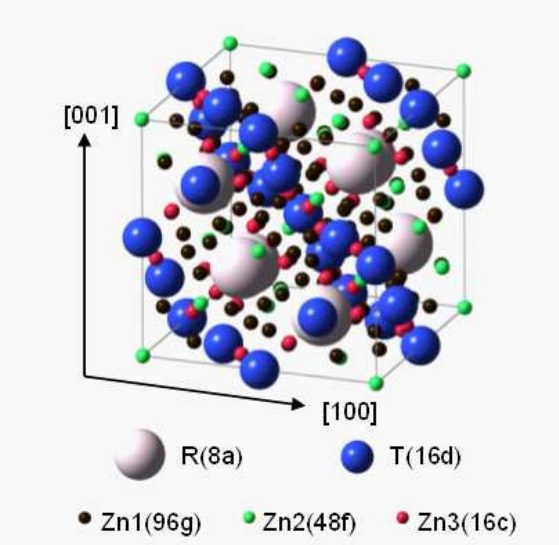

FIG. 1: (color online) The crystal structure of RT_2Zn_{20}. The thin lines outline the cubic unit cell. The unit cell dimension, a, is approximately 14 Å for the RT_2Zn_{20} families.

iron column members (with enhanced T_C values for T = Fe and Ru) and low temperature antiferromagnetic (AFM) transitions in the cobalt column members. Consistent with these results, we also found enhanced paramagnetism in the T = Fe and Ru of YT_2Zn_{20} analogues. For $GdFe_2Zn_{20}$ and $GdRu_2Zn_{20}$, magnetization measurements under hydrostatic pressure indicated that their enhanced FM transitions are not primarily associated with a steric effect. A model of Heisenberg moments embedded in a NFFL can be proposed as a way to understand the enhanced FM transitions. Band structure calculations were employed to explain that the remarkable differences in magnetic ordering for different transition metal members are a result of different d-band filling. In order to test this further, a series of pseudo-ternary compounds $Y(Fe_xCo_{1-x})_2Zn_{20}$ and $Gd(Fe_xCo_{1-x})_2Zn_{20}$ were made, characterized and found to manifest a clear, systematic and comprehensible evolution from normal, to nearly FM, metal, and from AFM state to high temperature FM state, respectively, associated with a change of the d-band filling as x varies from 0 to 1.

II. EXPERIMENTAL METHODS AND CALCULATION DETAILS

Single crystals of RT_2Zn_{20} (R = Gd, Y; T = Fe, Co, Ru, Rh, Os and Ir) were grown from a Zn-rich self flux.[3, 10] The initial concentration of starting elements (R:T:Zn) were 2: 4:

96 (T = Fe and Co), 1: 2: 97 (T = Ru, Rh), 1: 0.5: 98.5 (T = Os), and 0.75: 1.5: 97.75 (T = Ir). High purity, constituent elements were placed in alumina crucibles and sealed in quartz tubes under approximately 1/3 atmosphere of high purity Ar. Then the ampules were heated up to 1000 °C (T = Fe and Co), 1150 °C (T = Ru), 1100 °C (T = Rh), 1150 °C (T = Os and Ir), and cooled down to 600 °C, 850 °C, 700 °C, 750 °C respectively, at which point the remaining liquid was decanted. The cooling rates were 5 °C/hr (T = Fe, Co, Ru, Rh), 4 °C/hr (T = Os), and 2.5 °C/hr (T = Ir). Growths such as these often had only 2–3 nucleation sites per crucible and yielded crystals with typical dimensions of $7 \times 7 \times 7$ mm^3 or larger except for the Os compounds, which were significantly smaller (1–2 mm on one side). Residual flux and/or oxide slag on the crystal surfaces was removed by using diluted acid (0.5 vol. % HCl in H_2O for T = Fe, Co or 1 vol. % acetic acid in H_2O for T = Ru, Rh, Os and Ir). The samples were characterized by room temperature, powder X-ray diffraction measurements using Cu K_α radiation with Si ($a = 5.43088$ Å) as an internal standard. The lattice constants were obtained by using the Rietica, Rietveld refinement program.

Subsequent single crystal X-ray analyses were made using a STOE image plate diffractometer with Mo K_α radiation using the supplied STOE software[11]. The data were adjusted for Lorentz and polarization effects, and a numerical absorption correction was done. The structural solutions were refined by full-matrix least-squares refinement using Bruker SHELXTL 6.1 software package[12]. The atomic disorder in the crystals was checked by refining site occupancies.

The magnetization measurements under hydrostatic pressure were preformed in a piston-cylinder clamp-type pressure cell, made out of non-magnetic Ni-Co alloy MP35N, in the Quantum Design superconducting quantum interface device (SQUID) magnetometers. Pressure was generated in a Teflon capsule filled with 50:50 mixture of n-pentane and mineral oil. The pressure dependent, superconducting transition temperature of 6-N purity Pb was employed to determine the pressure at low temperatures.[13] The pressure cell design allows for the routine establishment of pressures in excess of 8 kbar at low temperatures.[14]

Measurements of the electrical resistivity were made by using a standard AC, four-probe technique. The samples were cut as bars, which typically had length 2–3 mm, parallel to the crystallographic [110] direction. AC electrical resistivity measurements were taken on these bars with $f = 16$ Hz, $I = 0.5$–0.3 mA in Quantum Design physical properties measurement system, PPMS-14 and PPMS-9 instrument ($T = 1.85$–310 K). Temperature

dependent specific heat measurements were also performed by using the heat capacity option of these Quantum Design instruments. DC magnetization was measured in Quantum Design SQUID magnetometers, in applied field $\leq$ 55 kOe or 70 kOe and in the temperature range from 1.85 K to 375 K.

In general, when making magnetization measurements on FM samples, some attention must be paid to the effects of demagnetizing fields.[15] However, this correction is small in the case of GdT_2Zn_{20} because of the diluted nature of the magnetic moments. Considering that the magnetization is mainly from the eight Gd^{3+} ions per unit cell, one estimates the maximum demagnetizing field as:

$$D_m(Max) = 4\pi \frac{8 \times 7\ \mu_B}{(14\ \mathring{A})^3} = 2380\ Oe. \quad (1)$$

Experimentally, in the measurements of magnetization isotherms near T_C, the demagnetizing field can introduce an error of T_C for plate-like shaped samples. To avoid this error, rod-like samples were measured with the applied magnetic field along their long axis. This minimized the demagnetizing factor and thereby the demagnetizing field.

The electronic structure was calculated using the atomic sphere approximation, tight binding, linear muffin-tin orbital (TB-LMTO-ASA) method[16, 17] with the experimental values of the lattice parameters and atomic positions from this work. The exchange-correlation term was calculated both within the local-spin-density approximation (LSDA) which was parameterized according to von Barth-Hedin[18], and the generalized gradient approximation (GGA) with the Perdew-Burke-Ernzerhof functional[19]. A mesh of 16 $\vec{k}$ points in the irreducible part of the Brillouin zone (BZ) was used. The $4f$ electrons of the Gd atoms were treated as polarized core states. Despite its apparent simplicity, this approach reproduces the electronic and magnetic properties of rare earth in good agreement with experiment.[20, 21] In order to reproduce the AFM ordering in $GdCo_2Zn_{20}$ the magnetic moments of two Gd atoms in the unit cell were aligned in opposite direction.

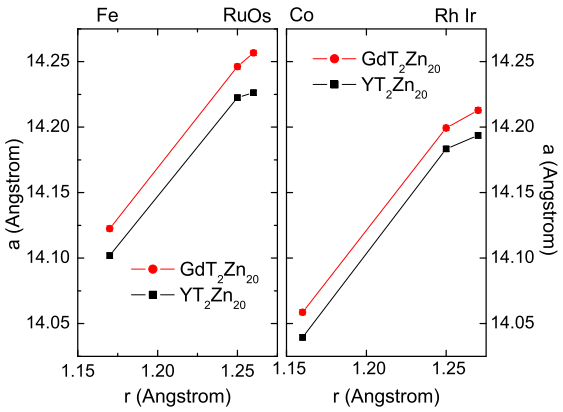

FIG. 2: (color online) The lattice constants (a) of GdT_2Zn_{20} and YT_2Zn_{20} versus the radius of the free, trivalent transition metal ion (r)[22].

III. RESULTS AND ANALYSIS

A. Structure refinements

Shown in Fig. 2, the lattice parameters, determined by the refinement of powder X-ray diffraction, increase as the transition metal varies from $3d$ to $5d$ for both of GdT_2Zn_{20} and YT_2Zn_{20}. The error bars, smaller than the symbols in the plot, were estimated from the standard variation of multiple measurement results on one batch of sample. In addition to the refinement of powder X-ray diffraction, the crystallographic atomic site occupancies and positions were refined using single crystal X-ray data on the crystals of $GdFe_2Zn_{20}$ and $GdRu_2Zn_{20}$. Shown in Table I, both compounds were found to be fully or very close to fully stoichiometric. The atomic site positions are very close to the isostructural compounds reported before[6]. It should be noted, though, that the similar atomic number values for Zn and Fe made it difficult to resolve possible mixed site occupancies.

B. GdT_2Zn_{20}(T = Fe, Co, Ru, Rh, Os and Ir)

Before discussing each of the GdT_2Zn_{20} compounds separately, an overview of their temperature and field dependent magnetization serves as a useful point of orientation. In Fig. 3 the temperature dependent magnetization (M) divided by applied field (H) reveals the primary difference between the Fe column members of this family and the Co column mem-

TABLE I: Atomic coordinates and refined site occupancies for $GdFe_2Zn_{20}$ and $GdRu_2Zn_{20}$; each of the unique crystallographic sites were refined individually.

Atom	Site	Occupancy	x	y	z
		$GdFe_2Zn_{20}$			
Gd	8a	1.013(12)	0.125	0.125	0.125
Fe	16b	1.01(2)	0.5	0.5	0.5
Zn1	96g	0.993(7)	0.0587(1)	0.0587(1)	0.3266(1)
Zn2	48f	0.997(9)	0.4893(1)	0.1250	0.1250
Zn3	16c	1.006(18)	0	0	0
		$GdRu_2Zn_{20}$			
Gd	8a	1.026(9)	0.125	0.125	0.125
Ru	16b	1.030(11)	0.5	0.5	0.5
Zn1	96g	0.988(5)	0.0589(1)	0.0589(1)	0.3260(1)
Zn2	48f	1.000(8)	0.4888(1)	0.1250	0.1250
Zn3	16c	0.962(15)	0	0	0

bers. For T = Fe, Ru and Os there is an apparent FM ordering (with remarkably high and moderately high values of T_C for T = Fe and Ru respectively), whereas for T = Co, Rh and Ir there is an apparent, low temperature AFM ordering.

The nature of the ordering is further confirmed by the low temperature, magnetization isotherms presented in Fig. 4. It should be noted that for each of the six GdT_2Zn_{20} compounds, the 1.85 K magnetization isotherms, measured with the applied field along [100], [110], [111] crystallographic directions, were found to be isotropic to within less than 5 %. This magnetic isotropy is not unexpected in the Gd-based intermetallics, in which the magnetism is mainly due to the pure spin contribution of the $4f$ shell of Gd^{3+}. For T = Fe, Ru and Os the magnetization is representative of a FM-ordered state with a rapid rise and saturation of the ordered moment in a field of the order of the estimated demagnetizing field (magnetic domain wall pinning being low in these single crystalline samples). For T = Co, Rh and Ir the field dependent magnetization data are consistent with AFM-ordered states that can be field stabilized to fully saturated states in large enough applied fields. This fully saturated state is observed for $GdCo_2Zn_{20}$ associated with a spin-flop transition

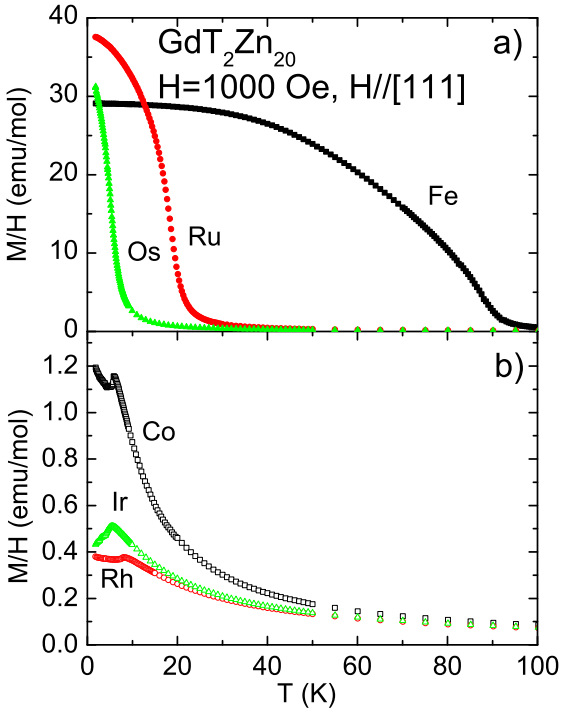

FIG. 3: (color online) Temperature dependent magnetization of GdT_2Zn_{20}, divided by applied field $H = 1000$ Oe.

near $H = 31$ kOe, whereas the maximum magnetic field in the equipment used (55 kOe) could not saturate the magnetic moment of the $GdRh_2Zn_{20}$ and $GdIr_2Zn_{20}$ samples. The measured saturated moments for T = Fe, Ru, Os and Co samples are clustered around the Hund's rule ground state value of Gd^{3+}, 7 μ_B.

Figure 5 presents temperature dependent H/M data for the six Gd based compounds. For this low magnetic field, H/M approximately equals inverse susceptibility $[1/\chi(T)]$ in the paramagnetic state. Except for $GdFe_2Zn_{20}$, the data sets of $1/\chi(T)$ of these compounds are linear and parallel to each other over the whole temperature range of the paramagnetic state, manifesting Curie-Weiss (CW) behavior, $\chi(T) = C/(T-\theta_C)$, where C is Curie constant and θ_C is paramagnetic Curie temperature. The same C value is extracted from the parallel lines gives the same effective moments($\mu_{eff} \simeq 8\ \mu_B$), close to the value of Hund's rule ground state of Gd^{3+}(7.94 μ_B), without any apparent contribution from local moments associated with the transition metal. This is consistent with the low temperature saturated moments, being close to the theoretical value, $\mu_{sat} = 7\ \mu_B$ (Fig. 4). In contrast, $1/\chi(T)$ of $GdFe_2Zn_{20}$ obeys a simple CW law only above ~ 200 K and evidently deviates from it at lower temperatures

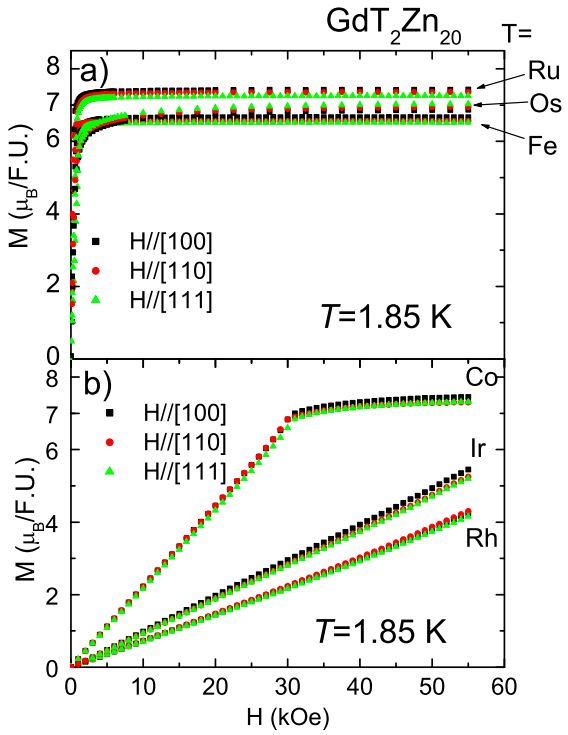

FIG. 4: (color online) Field dependent magnetization of GdT_2Zn_{20} at 1.85 K.

(see discussion below). Nevertheless, its high-temperature CW behavior yields μ_{eff} close to the others. The sign of the θ_C values is consistent with their magnetic ordering type, except for $GdCo_2Zn_{20}$, which manifests AFM order but a positive, albeit small, θ_C (Table II). This anomalous θ_C value for $GdCo_2Zn_{20}$ leads to a much larger susceptibility near the Néel temperature, $T_{\rm N}$, than T = Rh and Ir members (Fig. 3).

$GdFe_2Zn_{20}$ is the most conspicuously anomalous in its behavior. Figure 6 presents a blow up of the low field M/H data as well as the results of measurements of temperature dependent specific heat (C_p) and electrical resistivity (ρ) in zero applied magnetic field. The specific heat data manifest a clear anomaly at $T_{\rm C} = 85 \pm 1$ K [inset of Fig. 6(b)]. The resistivity data, although collected from a sample from different batch, show a clear break in slope (or maximum in $d\rho/dT$) at $T_{\rm C} = 84 \pm 2$ K. Determination of the ordering temperature from magnetization data requires a more detailed analysis. Figure 7 presents a plot of M^2 versus H/M (an Arrott plot)[23] from data collected on the same batch of sample used for C_p in the vicinity of $T_{\rm C}$. The isotherm that most closely goes linearly through the origin is the one closest to $T_{\rm C}$, giving a value 88 K. All of these measurements are consistent with

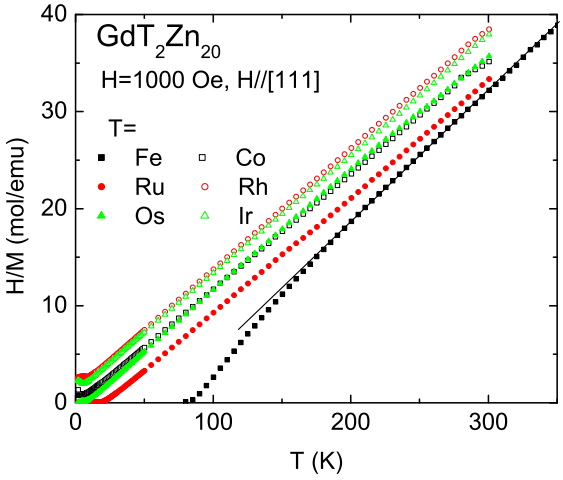

FIG. 5: (color online) Applied field ($H = 1000$ Oe) divided by the magnetizations of GdT_2Zn_{20} as a function of temperature. The solid line represents the high-temperature CW fit for $GdFe_2Zn_{20}$.

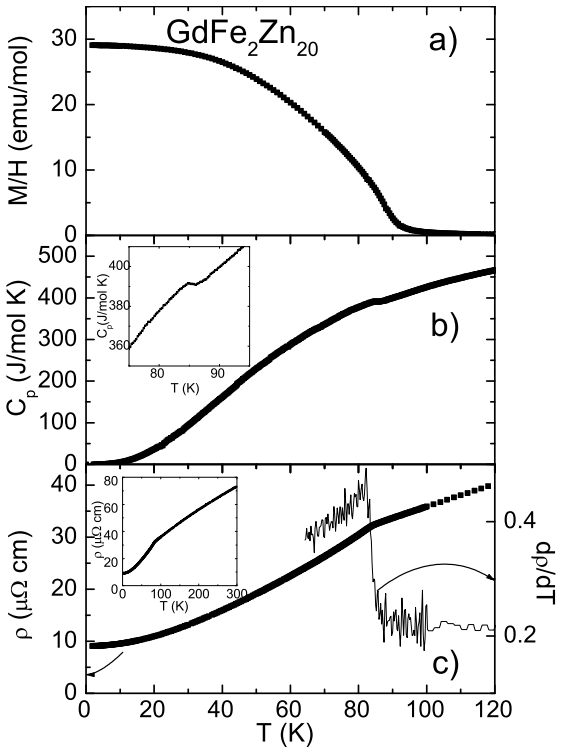

FIG. 6: (a) Temperature dependent magnetization (M) of $GdFe_2Zn_{20}$ divided by applied field ($H = 1000$ Oe); (b) specific heat (C_p); (c) resistivity (ρ)and its derivative respect to temperature ($d\rho/dT$). Inset in (b): detail of C_p data near T_C. Inset in (c) ρ over whole temperature range, 2 K - 300 K.

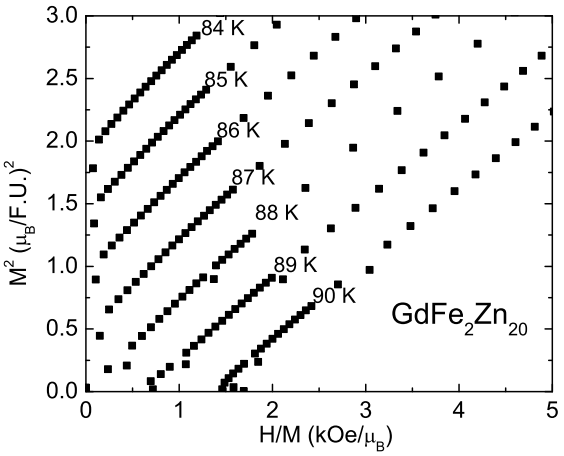

FIG. 7: Arrott plot for $GdFe_2Zn_{20}$.

transition temperature near 86 K. It should be noted though, that T_C values for different batch of samples can vary by as much as ±3 K [3], even though the single-crystal X-ray measurements do not suggest evident crystallographic difference.

$GdRu_2Zn_{20}$ also manifests a relatively high FM ordering temperature. Figures 8(b, c) present temperature dependent specific heat and electrical resistivity measurements on $GdRu_2Zn_{20}$ in zero applied magnetic fields, both of which show clear evidence of ordering with $T_C = 20 \pm 1$ K. Figure 9 shows that, similar to $GdFe_2Zn_{20}$, the T_C of $GdRu_2Zn_{20}$ can be inferred from an Arrott plot analysis. These measurements were performed on samples from the same batch and the different methods for determining T_C agree to within ±1 K difference.

$GdOs_2Zn_{20}$ appears to order ferromagnetically at a T_C value as low as the Néel temperatures found for the Co column members of the GdT_2Zn_{20} family (see below). As shown in Fig. 10(b) and (c), the specific heat and resistivity data manifest features consistent with a magnetic phase transition near 4 K. However, the C_p data, with a broad shoulder above this temperature, does not manifest a standard λ-type of feature and may indicate a distribution of T_C values or multiple transitions. The Arrott plot for $GdOs_2Zn_{20}$, although having non-linear, isothermal curves, is also consistent with a FM transition between 4 K and 4.5 K (Fig. 11). Such a non-linear feature in the isothermal curves is also found in ref.[24, 25], and may be associated with complex magnetic phenomenon in the critical region, rather than one simple, clearly defined, Landau type, 2nd order phase transition.

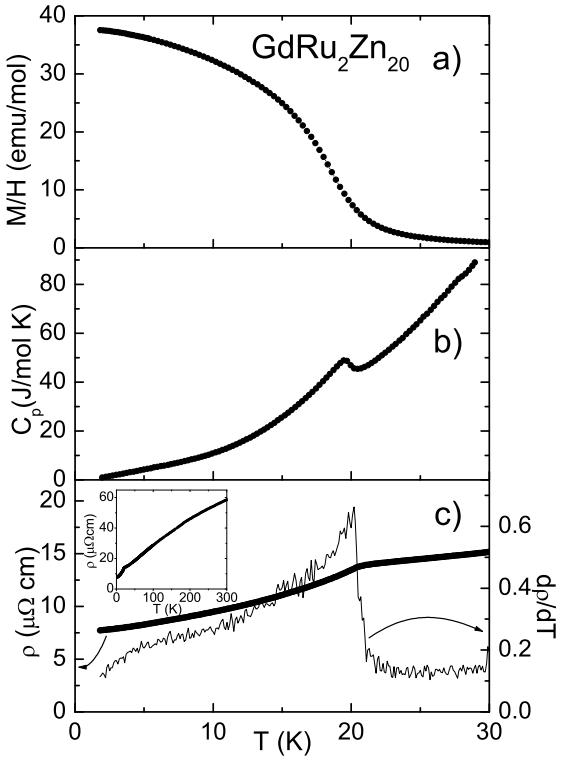

FIG. 8: (a) Temperature dependent M/H for $GdRu_2Zn_{20}$ ($H = 1000$ Oe); (b) C_p; (c) ρ and $d\rho/dT$. Inset in (c): ρ over whole temperature range.

In contrast to the Fe column compounds, the Co column compounds all appear to order antiferromagnetically with the values of T_N between 4 and 7 K. Figures 12, 13 and 14 present the low temperature magnetic susceptibility, specific heat and electrical resistivity data for $GdCo_2Zn_{20}$, $GdRh_2Zn_{20}$ and $GdIr_2Zn_{20}$ respectively. In addition to these data, $d(\chi(T)T)/dT$ [26] and $d\rho/dT$ [27] have been added to the susceptibility and resistivity plots respectively. $GdCo_2Zn_{20}$ and $GdRh_2Zn_{20}$ manifest clear λ-type anomalies in their temperature dependent specific heat, with similar features appearing in their $d\rho/dT$ and $d(\chi(T)T)/dT$ data. From these thermodynamic and transport data we infer T_N of 5.7 K and 7.6 K for $GdCo_2Zn_{20}$ and $GdRh_2Zn_{20}$ respectively. $GdIr_2Zn_{20}$ shows a somewhat broader feature at $T_N = 4$ K and there may be a lower temperature transition near 2 K indicated in the magnetization data, although this is not clearly supported by corresponding features in either specific heat or resistivity data. A summary of the thermodynamic and transport measurements on the six GdT_2Zn_{20} compounds is presented in Table II.

A logical question that comes to mind when comparing T_C for the Fe column members

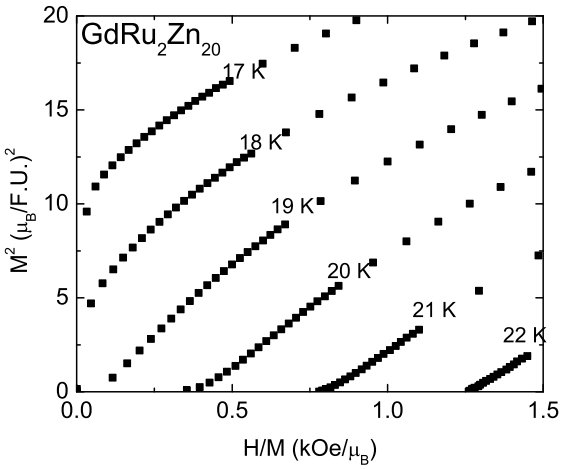

FIG. 9: Arrott plot for $GdRu_2Zn_{20}$.

TABLE II: Residual resistivity ratio, $RRR = \frac{R(300K)}{R(2K)}$; paramagnetic Curie temperature, θ_C and effective moment, μ_{eff} (from the CW fit of $\chi(T)$ from 100 K to 300 K, except for $GdFe_2Zn_{20}$; see text for details); magnetic ordering temperature, T_{mag}; and saturated moment at 55 kOe along [111] direction, μ_{sat} on GdT_2Zn_{20} compounds (T = Fe, Ru, Os, Co, Rh, Ir).

T	Fe	Ru	Os	Co	Rh	Ir
RRR	8.1	7.6	5	12.8	12.8	15.7
θ_C, K	46	23	3	3	-10	-8
μ_{eff}, μ_B	7.9	8.2	8.1	8.2	8.0	8.1
T_{mag}, K	86	20	4.2	5.7	7.7	4.2, 2.4[a]
μ_{sat}, μ_B	6.5	7.25	6.9	7.3		

[a]two magnetic transitions were found

with the lattice parameter data shown in Fig. 2 is whether the drop in T_C as the transition metal moves down the column is associated with a steric effect. This can be addressed experimentally by measurements of T_C under hydrostatic pressure. Figure 15 presents low field magnetization for $GdFe_2Zn_{20}$ and $GdRu_2Zn_{20}$ under pressures up to 7 kilobar. The application of pressure suppresses the ferromagnetically ordered state in both compounds and the pressure dependence of $T_{10\%}$ (the temperature where the magnetization equals 10% of maximum magnetization and used as a caliper of T_C) of each compound is plotted in Fig.

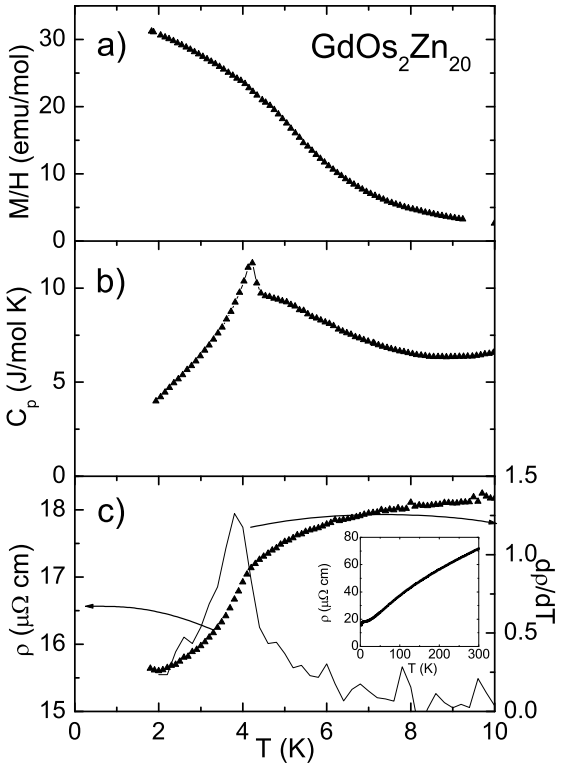

FIG. 10: (a) Temperature dependent M/H for $GdOs_2Zn_{20}$ (H = 1000 Oe); (b) C_p; (c) ρ and $d\rho/dT$. Inset in (c): ρ over whole temperature range.

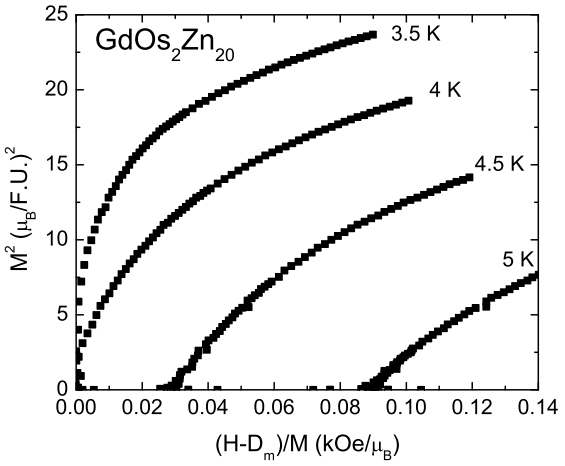

FIG. 11: Arrott plot for $GdOs_2Zn_{20}$. The demagnetizing field D_m can not be ignored for this low T_C, and was estimated from the geometric factor of the sample ($D \sim 0.03$).

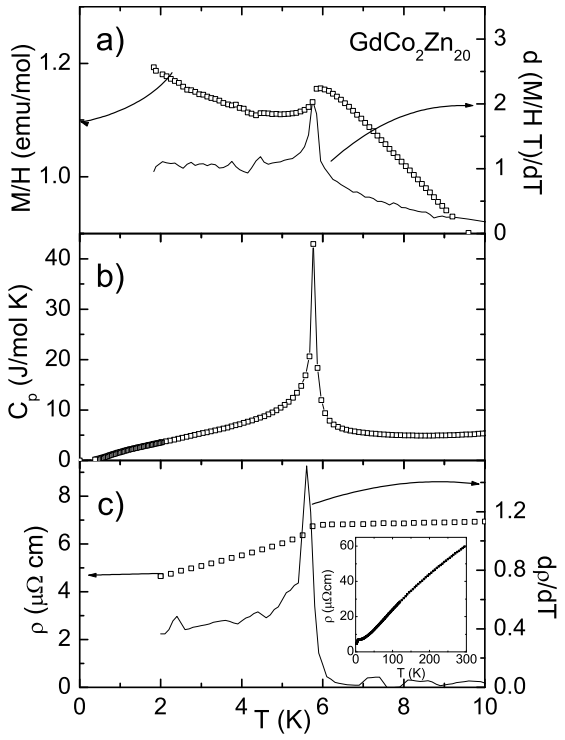

FIG. 12: (a) Temperature dependent susceptibility (χ) and $d(\chi T)/dT$ of $GdCo_2Zn_{20}$; (b) C_p; (c) ρ and $d\rho/dT$. Inset in (c): ρ over whole temperature range.

16. The fact that both compounds manifest a suppression of T_C with increasing pressure indicates that the difference between $GdFe_2Zn_{20}$ and $GdRu_2Zn_{20}$ is not primarily a steric one. Approximating the bulk modulus of these compounds to be a generic 1Mbar, one can estimate that $GdRu_2Zn_{20}$ under 10 kbar hydrostatic pressure will have its lattice parameter reduced by 0.03 Å(25% of the difference between the lattice parameter of $GdFe_2Zn_{20}$ and $GdCo_2Zn_{20}$). If the cause of the T_C suppression was purely steric, such a change in lattice parameter should (at the very least) result in a dramatic increase in the T_C values of $GdRu_2Zn_{20}$ rather than the gradual suppression observed.

C. YT_2Zn_{20}(T = Fe, Co, Ru, Rh, Os and Ir)

In order to better understand the behavior of $GdFe_2Zn_{20}$ and $GdRu_2Zn_{20}$ with respect to the rest of the GdT_2Zn_{20} compounds, it is useful to examine the properties of the nonmagnetic analogues: the YT_2Zn_{20} compounds. The temperature dependent magnetization data

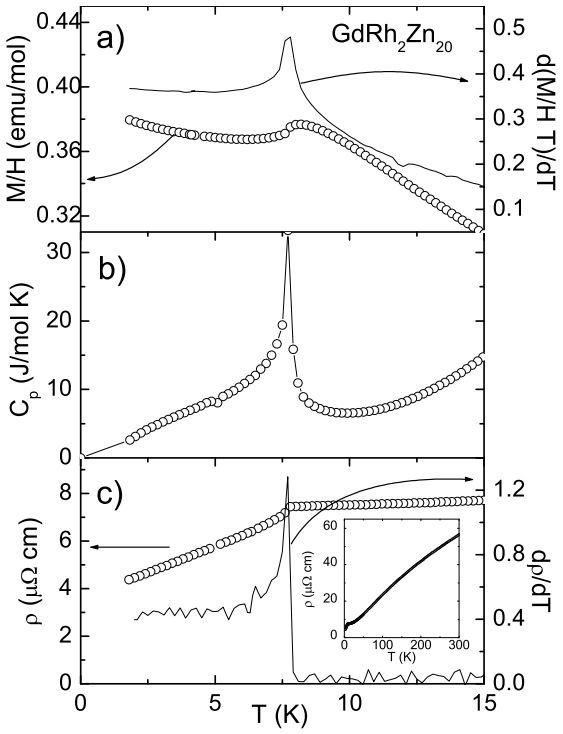

FIG. 13: (a) Temperature dependent χ and $d(\chi T)/dT$ of $GdRh_2Zn_{20}$; (b) C_p; (c) ρ and $d\rho/dT$. Inset in (c): ρ over whole temperature range.

(divided by applied field) and the low temperature magnetization isotherms for these six compounds are presented in Fig. 17 and Fig. 18, respectively. YFe_2Zn_{20} and YRu_2Zn_{20} have a greatly and intermediately enhanced paramagnetic signals respectively, whereas the rest of the materials manifest the ordinary weak, either paramagnetic or diamagnetic, response, anticipated for non-moment bearing intermetallic compounds.

Measurements of low temperature specific heat (plotted as C_p/T versus T^2 in Fig. 19) also indicate a clear difference between YFe_2Zn_{20}, YRu_2Zn_{20} and the other members of the YT_2Zn_{20} series: enhanced values of the electronic specific heat being found for T = Fe and Ru. As previously reported[3], YFe_2Zn_{20} can be thought of as being close to the Stoner limit. The simplest way to see this is to recall that, in this limit, whereas the Pauli paramagnetism is enhanced by a factor $(1-Z)^{-1}$, the electronic specific heat is not[28]. This means that the term Z in the enhancement factor can then be inferred from the experimentally determined, low temperature values of γ_0 and χ_0. In common units

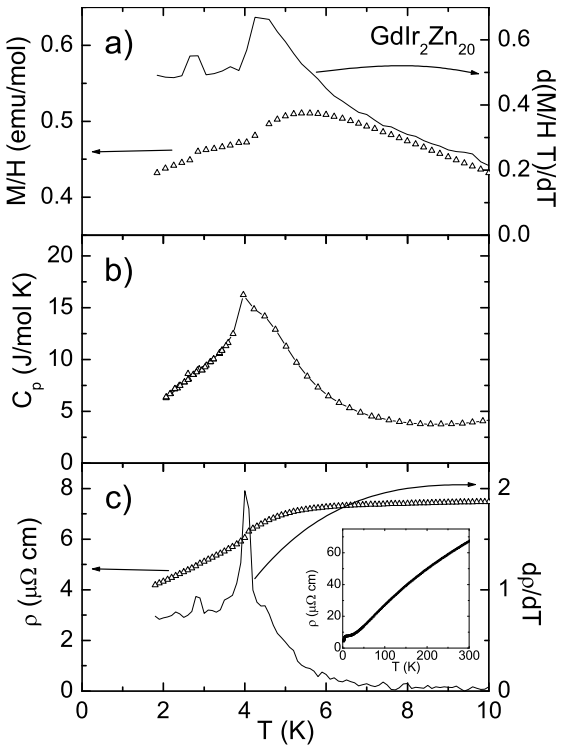

FIG. 14: (a) Temperature dependent χ and $d(\chi T)/dT$ of $GdIr_2Zn_{20}$; (b) C_p; (c) ρ and $d\rho/dT$. Inset in (c): ρ over whole temperature range.

$$Z = 1 - 1.37 \times 10^{-2} \frac{\gamma_0(J/molK^2)}{\chi_{0-dia}(emu/mol)} \tag{2}$$

where χ_{0-dia} equals χ_0 with the core diamagnetism subtracted.

Giving the core diamagnetism values(-2.3×10^{-4}emu/mol for YFe_2Zn_{20} and YCo_2Zn_{20}, -2.5×10^{-4}emu/mol for YRu_2Zn_{20} and YRh_2Zn_{20}, and -2.9×10^{-4}emu/mol for YOs_2Zn_{20} and YIr_2Zn_{20})[29], Z can be inferred to be 0.88 and 0.67 for YFe_2Zn_{20} and YRu_2Zn_{20} respectively (Table III). For reference, this can be compared to $Z = 0.83$ and 0.57 for elemental Pd and Pt respectively[30], which are thought to be canonical examples of NFFL. These enhanced Z values indicate that YRu_2Zn_{20}, and particular YFe_2Zn_{20} are extremely close to the Stoner limit ($Z = 1$). In contrast, the Z values of the rest of the members are less than 0.5, which is comparable with the estimated value of the canonical example of 'normal metal', Cu, $Z = 0.29$ [31]. It is worth to notice that, during the estimation of the Z values, the contribution from the Landau diamagnetism is ignored. Inversely proportional to the square of the effective mass of the conduction electrons[32], the Landau diamagnetic con-

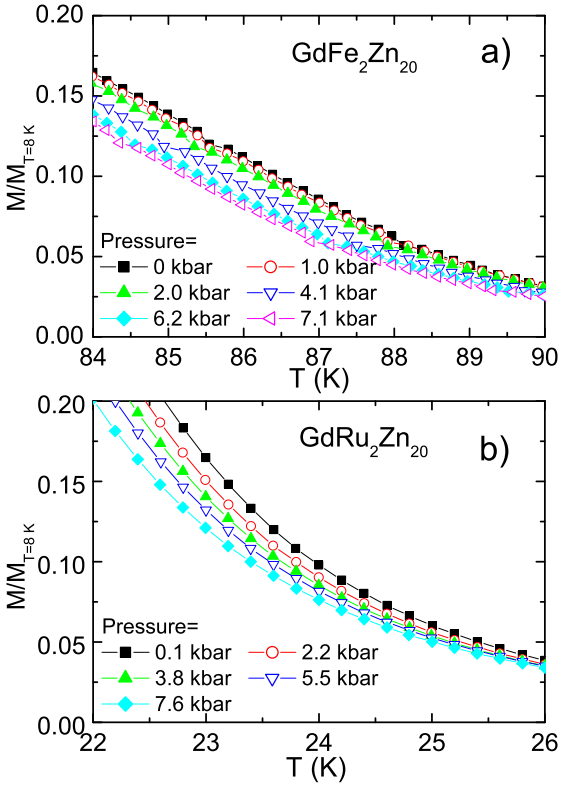

FIG. 15: (color online) Magnetization of (a): $GdFe_2Zn_{20}$ and (b): $GdRu_2Zn_{20}$ in applied field ($H = 1000$ Oe) under different hydrostatic pressure.

tribution becomes more significant for those members which have smaller γ_0 values. Thus, based on the thermodynamic measurements, the Pauli susceptibility values, even after the core diamagnetism correction, are still under-estimated. Due to this uncertainty, the Pauli susceptibility values after the core diamagnetism correction for YOs_2Zn_{20} and YRh_2Zn_{20}, albeit positive, are still less than the un-enhanced values ($Z = 0$) corresponding to their γ_0.

D. Electronic Structure

Band structure calculations, performed on the representative, non-local moment members, YT_2Zn_{20} (T = Fe, Co and Ru), as well as their local moment analogues, GdT_2Zn_{20}, can help us to understand their diverse magnetic properties further. Figure 20 shows the result of the total and partial density of states (DOS) for each element for YFe_2Zn_{20}. At the Fermi level, E_F, the total DOS manifests a sharp peak, leading to the relatively large

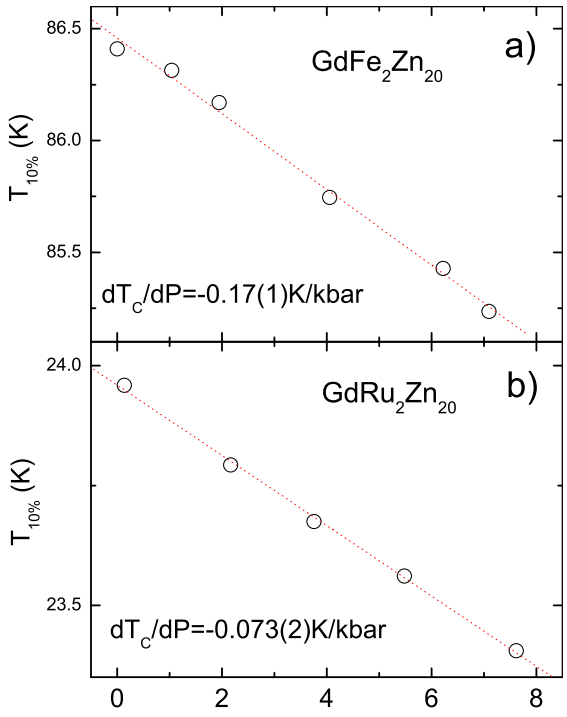

FIG. 16: Pressure dependent $T_{10\%}$ (inferred as T_C) of $GdFe_2Zn_{20}$ and $GdRu_2Zn_{20}$. The dash lines are the linear fits of the data.

DOS at Fermi level ($N(E_F)$, see Table IV), and therefore large band contributed electronic specific heat, $\gamma_{band} = 30.6$ mJ/mol K^2. This result is consistent with the experimentally measured electronic specific heat, γ_0 with a large mass enhanced factor, $\lambda = 0.73$, if one assumes $\gamma_0 = (1+\lambda)\gamma_{band}$. The peak-shape DOS at E_F is not unusual for the NFFL systems: similar calculation results have been obtained for Pd[33], YCo_2[34] and Ni_3Ga[35] by using similar techniques. The large peak at about -7 eV corresponds to totally filled d-states of Zn atoms. Figure 20 also shows significant contribution of Zn atoms' electronic states to the total DOS in the whole energy spectrum, whereas the Fe atoms' electronic states are mostly localized in the vicinity of E_F, although they are dilute in this compound (1/10 of Zn). Table IV shows that the partial DOS of Fe at E_F is in between the values for elemental Pd and Fe (before band splitting), the canonical examples of nearly ferromagnet and 'strong' ferromagnet systems. This result indicates that YFe_2Zn_{20} indeed may be even closer the Stoner criterion than Pd. The total DOS at E_F mainly corresponds to the hybridization of the $3d$-band of Fe and p-band of Zn; the $4d$-band of Y, although hybridized with the other

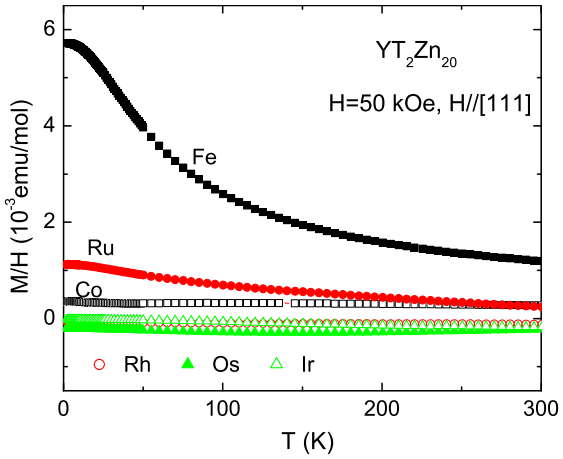

FIG. 17: (color online) Temperature dependent magnetization of YT_2Zn_{20} under applied field $H = 50$ kOe.

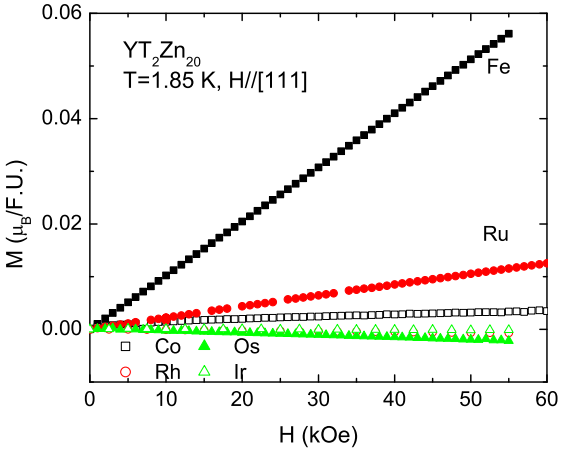

FIG. 18: (color online) Field dependent magnetization of YT_2Zn_{20} at 1.85 K.

two, contributes significantly less (Fig.20).

The dominant effect of the *d*-band filling on the magnetic properties of YT_2Zn_{20}, manifests itself clearer if one compares the electronic structure of the three YT_2Zn_{20} compounds: T= Fe, Co and Ru (Fig. 21). In Fig. 21, the total and Co-partial DOS of YCo_2Zn_{20} represents behavior similar to the YFe_2Zn_{20} analogues, whereas E_F is shifted 0.3 eV higher by adding 2 more valence electrons per formula unit. This similarity indicates that the difference in the electronic structure of YFe_2Zn_{20} and YCo_2Zn_{20} can be considered in terms of the rigid band approximation. On the other hand, the electronic structure of YRu_2Zn_{20} has

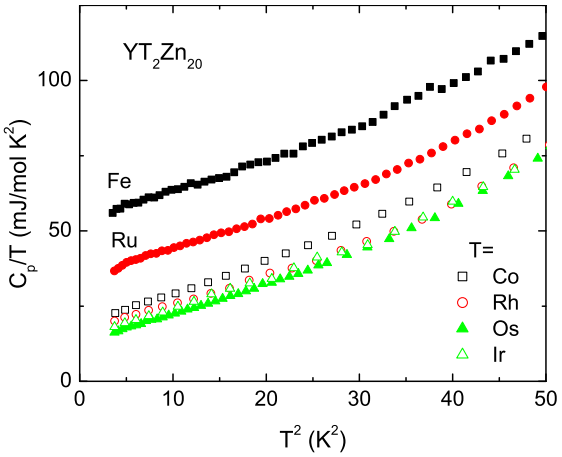

FIG. 19: (color online) Low temperature specific heat of YT_2Zn_{20}.

TABLE III: Low temperature susceptibility, χ_0; and the values after core diamagnetism correction, χ_{0-dia}; linear coefficient of the specific heat, γ_0; and the Stoner enhancement factor, Z on YT_2Zn_{20} compounds (T = Fe, Ru, Os, Co, Rh, Ir).

T	Fe	Ru	Os	Co	Rh	Ir
$\chi_0{}^a$,	5.73	1.14	-0.256	0.212	-0.076	-0.034
χ_{0-dia},	5.96	1.39	0.034	0.442	0.174	0.256
$\gamma_0{}^b$	53	34	12.4	18.3	16.4	14.1
θ_D, K	123	124	125	121	127	124
Z^c	0.88	0.67	-	0.43	-	0.24

[a]Taken as $\frac{M(50\ kOe)-M(30\ kOe)}{20\ kOe}$,in unit 10^{-3}emu/mol
[b]in unit mJ/molK^2
[c]Eqn. 2 is invalid for T = Os and Rh; see text

the same Fermi level position as YFe_2Zn_{20} because of the same valence electron filling. However, its total, and partial-Ru, DOS are lower than those for YFe_2Zn_{20}. This difference is not unexpected, since the $4d$ band is usually broader than the $3d$ band in the electronic structure of intermetallics. Calculated $N(E_F)$ of YCo_2Zn_{20} is half of the value of YFe_2Zn_{20}, whereas the value of YRu_2Zn_{20} is slightly larger than YCo_2Zn_{20} (Table IV).

The electronic structure calculation of the three GdT_2Zn_{20} analogues, based on the treatment of $4f$ electrons in core states, can help to understand the effect of a submerging Gd^{3+}

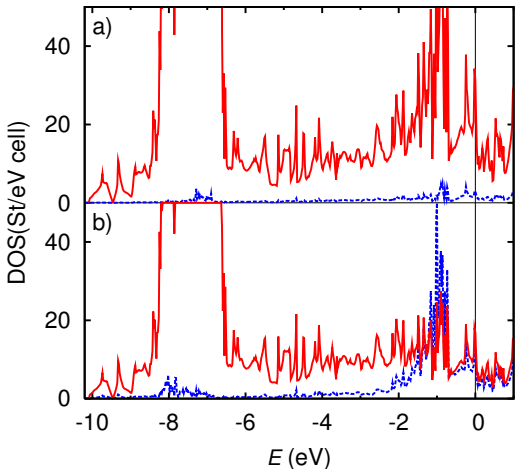

FIG. 20: (color online) The DOS of YFe_2Zn_{20} (in St/eV cell) and partial DOS (in St/eV cell). E_F corresponds to zero energy. The red color solid line on (a) corresponds to total DOS and blue dashed - to Y atoms PDOS. The red color solid line on (b) corresponds to PDOS of Zn and blue dashed - to Fe atoms PDOS.

local moment in these electronic backgrounds (Y analogues). Our calculations demonstrate that, in the ordered state, Gd and the transition metal carry magnetic moments (see Table IV). Magnetic moments of Gd atoms are about 7.4 μ_B for FM ordered compounds and 7.3 μ_B for AFM ordered compound, significantly smaller compared to elemental Gd result[20, 21], 7.6 μ_B. The magnetic moment additional to the Hund's value (7 μ_B) comes from the polarization of Gd's p and d states by magnetic $4f$ electrons. The negative coupling between Gd and transition metals induces magnetic moments on these atoms in direction opposite to the Gd magnetic moment. In agreement with the high DOS of Fe atoms in YFe_2Zn_{20}, the induced magnetic moment on Fe atoms, -0.84 μ_B, is the largest among all series. The smaller DOS of Ru atoms in YRu_2Zn_{20} compound correlates with a smaller induced magnetic moment on Ru in $GdRu_2Zn_{20}$: -0.04 μ_B. The induced magnetic moment on Co is zero because of the compensation of interactions with Gd in AFM $GdCo_2Zn_{20}$. The calculated total magnetic moment, 7.25 μ_B, 6.53 μ_B and 7.30 μ_B for GdT_2Zn_{20} (T = Co, Fe and Ru respectively), are in good agreement with the experimental values, 7.3 μ_B, 6.5 μ_B and 7.25 μ_B (see Table II). The DOS for $GdFe_2Zn_{20}$ [Fig. 22(a)] demonstrates a significant splitting between occupied and empty $3d$ states of Fe, in agreement with sizable Fe magnetic moments, whereas this splitting is almost negligible in case of Ru based compounds [Fig.

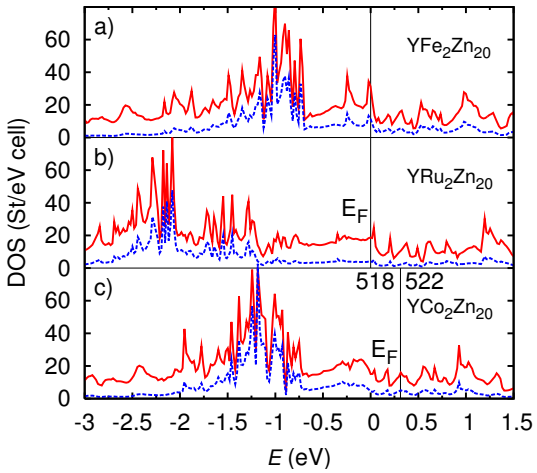

FIG. 21: (color online) The DOS of YFe_2Zn_{20} (a), YRu_2Zn_{20} (b) and YCo_2Zn_{20} (c) near E_F (in St/eV cell) shown by red solid line and PDOS of Fe, Ru and Co atoms (blue dashed line) (in St/eV cell). E_F is shown by vertical lines. 518 and 522 corresponds to number of valence electrons in the unit cell calculated in the rigid band approximation from the DOS of YFe_2Zn_{20}.

22(b)].

E. $Gd(Fe_xCo_{1-x})_2Zn_{20}$ and $Y(Fe_xCo_{1-x})_2Zn_{20}$

Based on the distinct difference between the RFe_2Zn_{20} and RCo_2Zn_{20} compounds and motivated by the band structural calculations, a systematic study of $R(Fe_xCo_{1-x})_2Zn_{20}$ for R = Gd and Y was made. The same growth conditions for T = Fe and Co samples further facilitates such a study of the effects of $3d$ band filling, as well as proximity to the Stoner limit, on the magnetic ordering found in $GdFe_2Zn_{20}$. In order to check x of $Gd(Fe_xCo_{1-x})_2Zn_{20}$ and $Y(Fe_xCo_{1-x})_2Zn_{20}$, Energy Dispersive Spectra (EDS) measurements, a direct method to determine the elements concentrations, and powder X-ray diffraction measurements were employed. Figure 23 presents EDS measurement results for the Gd series, and the lattice constants for both series. The linear variation of lattice constants with x for both series is compliant with Vegard's law, which is consistent with the results of EDS. Due to these results; the nominal x value is used from this point onward.

Figure 24 shows the magnetization divided by the applied field as a function of temperature for $Gd(Fe_xCo_{1-x})_2Zn_{20}$, which indicates FM ordering for $x \geq 0.25$. As x is increased

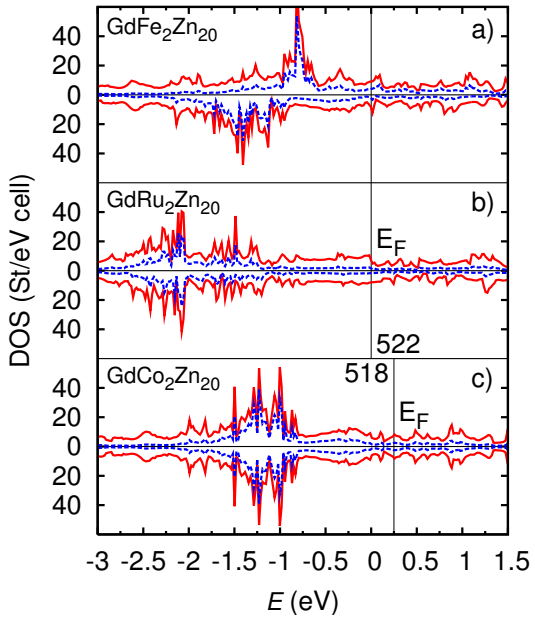

FIG. 22: (color online) The red solid line corresponds to DOS of FM-ordered $GdFe_2Zn_{20}$ (a), FM-ordered $GdRu_2Zn_{20}$ (b) and AFM one $GdCo_2Zn_{20}$ (c) near E_F (in St/eV cell) and partial DOS of Fe, Ru and Co atoms (blue dashed line) (in St/eV atom). E_F is shown by vertical lines. 518 and 522 corresponds to number of valence electrons in the unit cell calculated in the rigid band approximation from the DOS.

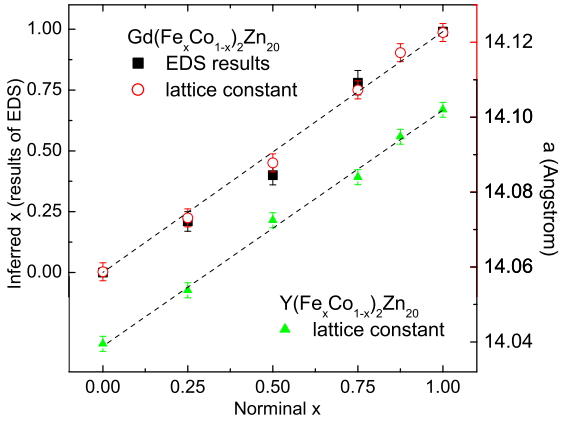

FIG. 23: (color online) Lattice constants of the series of $Gd(Fe_xCo_{1-x})_2Zn_{20}$ (open circle) and $Y(Fe_xCo_{1-x})_2Zn_{20}$ (solid triangle). Fe concentration of $Gd(Fe_xCo_{1-x})_2Zn_{20}$ series inferred from EDS measurements (solid square).

TABLE IV: The calculated DOS in St/eV cell ($N(E_F)$), averaged DOS per one atom ($N(E_F)/N_{atoms}$), partial DOS at transition metal atom ($N_T(E_F)$) and magnetic moment in μ_B for Gd and transition metal, T, in GdT_2Zn_{20} compounds.

Compound	$N(E_F)$	$N(E_F)/N_{atoms}$	$N_T(E_F)$	Magnetic Moment	
				Gd	T
Pt (elemental)	2.2	2.2	2.2		
Pd (elemental)	2.6	2.6	2.6		
Fe (elemental)	3.5	3.5	3.5		
YCo_2Zn_{20}	16.32	0.35	1.28		
YFe_2Zn_{20}	31.35	0.68	2.86		
YRu_2Zn_{20}	18.72	0.41	1.0		
$GdCo_2Zn_{20}$	14.92			7.25	0.00
$GdFe_2Zn_{20}$	17.95			7.37	-0.84
$GdRu_2Zn_{20}$	17.15			7.34	-0.04

from 0 to 1, the polarizability of the electronic background [$Y(Fe_xCo_{1-x})_2Zn_{20}$] increases, and there is a monotonic, but super-linear increase in T_{mag} (inset of Fig. 24), which is, reminiscent of the x dependent of Z inferred from measurements on $Y(Fe_xCo_{1-x})_2Zn_{20}$.[3] Clearer evidence of the FM ground states for $x \geq 0.25$ is present in the low temperature magnetization isotherms (Fig. 25). The saturated moment extracted from the magnetization values, under 55 kOe applied field along [111] crystallographic direction, varies monotonically from the slightly enhanced value of 7.3 μ_B for $GdCo_2Zn_{20}$ to the slightly deficient value of 6.5 μ_B for $GdFe_2Zn_{20}$.

IV. DISCUSSION

The band structure calculation indicates that, with same structure and similar lattice parameters, the diverse magnetic properties of GdT_2Zn_{20} and YT_2Zn_{20} are mainly dependent on the d-band conduction electrons from the transition metal site. The different d-band filling of the Fe column members and the Co column members is associated with the different sign of the magnetic coupling of Gd^{3+} local moments, and thereupon the different type of the

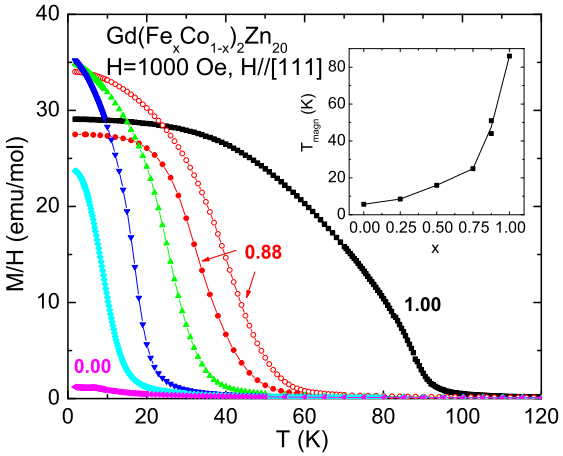

FIG. 24: (color online) M/H of $Gd(Fe_xCo_{1-x})_2Zn_{20}$ series versus temperature for $x = 1.00$, 0.88, 0.75, 0.50, 0.25 and 0 from right to left. Note data from two samples of $x = 0.88$ are shown. Inset: magnetic phase transition temperatures for $Gd(Fe_xCo_{1-x})_2Zn_{20}$.

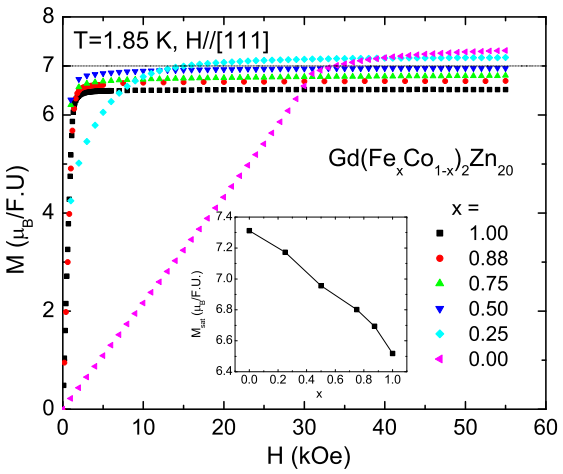

FIG. 25: (color online) Low temperature ($T = 1.85$ K) magnetization versus applied field for the series of $Gd(Fe_xCo_{1-x})_2Zn_{20}$. Inset: saturated moments as a function of x.

magnetic ordering. Furthermore, the high and intermediately high $N(E_F)$ of $3d$ and $4d$ subbands of Fe and Ru, respectively, are associated with the strongly correlated electronic state of YFe_2Zn_{20} and YRu_2Zn_{20}, as well as the strong coupling between the Gd^{3+} local moments in $GdFe_2Zn_{20}$ and $GdRu_2Zn_{20}$, and therefore the high magnetic ordering temperatures. The negative induced moment on Fe site is not unexpected in intermetallic systems consisting of a heavy rare earth and an over-half-filled, $3d$ transition metal[1, 36], which can be understood

in terms of the hybridization between the $3d$ electrons of transition metal and the $5d$ electrons of the rare earth[37].

In addition to the electronic structure calculation, the remarkable high-temperature FM ordering of $GdFe_2Zn_{20}$ and $GdRu_2Zn_{20}$ can be understood in the conceptually simple context of the large Heisenberg moments, associated with the Gd^{3+} ion ($\mathbf{S} = 7/2$), being embedded in the NFFL associated with YFe_2Zn_{20} and YRu_2Zn_{20}. This framework has been employed to understand the anomalously high temperature FM ordering in some systems of local moments in NFFL hosts, such as dilute Fe, Co, or Gd in Pd or Pt[38, 39], or RCo_2(R = Gd - Tm)[40, 41]. In these systems, the itinerant electrons of the host (Pd, Pt or YCo_2) are polarized by the local moments (Fe, Co ions or R^{3+} ions), strongly couple them, and result in high-temperature, local moments ordering and induced moment of themselves.

The substitutional series of $Gd(Fe_xCo_{1-x})_2Zn_{20}$ and $Y(Fe_xCo_{1-x})_2Zn_{20}$ provide the versatility to study the correlation between the local moments and the high polarizable host. When x is varied from 0 to 1, by tuning of the d-band filling, the inferred values of Z for the $Y(Fe_xCo_{1-x})_2Zn_{20}$ series, representing to some extent the polarizability, increase superlineally from 0.43 to 0.88,[3] giving rise to the highly non-linear increase of the magnetic ordering temperature for the $Gd(Fe_xCo_{1-x})_2Zn_{20}$ series (Fig. 24). This correspondence between the Z values and the magnetic ordering temperatures is even consistent with the T_C value for $GdRu_2Zn_{20}$, although the itinerant electrons of the transition metal are $4d$, not $3d$. Given $Z = 0.67$ for YRu_2Zn_{20}, a similar Z-value of the host is between $x = 0.5$ and 0.75 for $Y(Fe_xCo_{1-x})_2Zn_{20}$.[3] The T_C value of $GdRu_2Zn_{20}$ is also between the T_C values for $x = 0.5$ and 0.75 $Gd(Fe_xCo_{1-x})_2Zn_{20}$.

This conceptually simple framework can also help to understand the curious temperature dependence of the $1/\chi(T)$ data for $GdFe_2Zn_{20}$. Figure 26(a) shows the temperature dependent H/M in applied field ($H = 1000$ Oe), with a dash line presenting the CW fit above 250 K. As shown before, the fit gives the value of the effective moment ($\mu_{eff} = 7.9\ \mu_B$), comparable with the effective moment of $4f$ electrons of Gd^{3+} in Hund's ground state. The deviation from the CW law below 250 K has been explained as a result of temperature dependent coupling between Gd^{3+} local moments by means of strongly polarizable electronic background[3]. Assuming a constant μ_{eff}, one can extract the temperature dependence of θ_C from the $1/\chi$ data. As shown in Fig. 26(b), θ_C essentially constant (~ 45 K) above 275 K; then increases monotonically as temperature decrease, tracking $\chi(T)$ of YFe_2Zn_{20} (Fig.

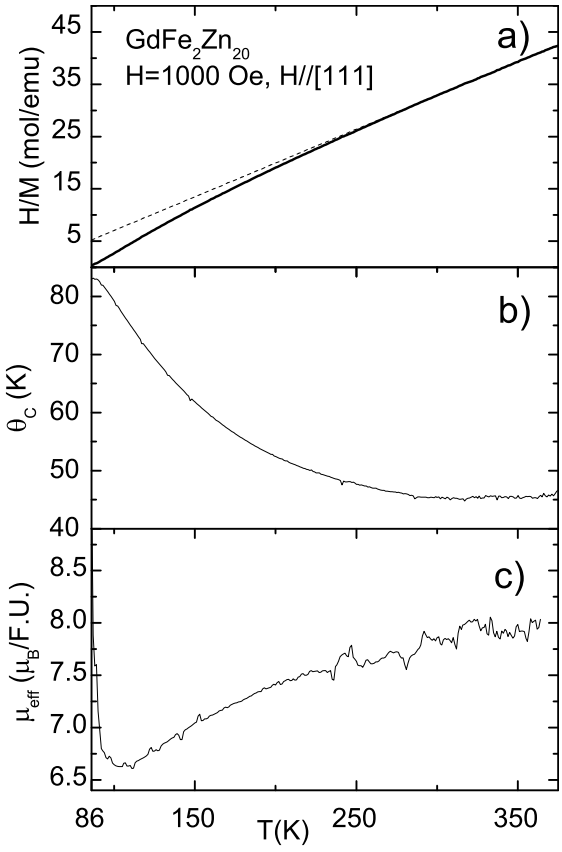

FIG. 26: (a): H/M (H = 1000 kOe) of $GdFe_2Zn_{20}$ as a function of temperature. The dash line represents the Curie-Weiss fit above 250 K. (b): temperature varied θ_C. (c): temperature varied μ_{eff}. (See text)

17).

The correlation of the temperature dependent χ and the polarizability of electronic background, can also be seen in the susceptibility of $Gd(Fe_xCo_{1-x})_2Zn_{20}$ series. Figure 27(a) presents temperature dependent H/M under the applied field H = 1000 Oe. Linear and parallel to each other at high temperature region, the data sets start to deviate at lower temperature, especially for large x. Similar to discussed before, the temperature dependent θ_C values were extracted with the assumption of invariant μ_{eff}. Figure 27(b) shows that θ_C varies strongly, much weakly and negligibly as $x = 1$, 0.88 and ≤ 0.75, respectively. For each x, the variation of θ_C tracks $\chi(T)$ of the $Y(Fe_xCo_{1-x})_2Zn_{20}$ series.[3]

An alternative method of analyzing the $\chi(T)$ data assumes that some induced moment exists above T_C and is aligned locally anti-parallel to the Gd moment (in essence forming a

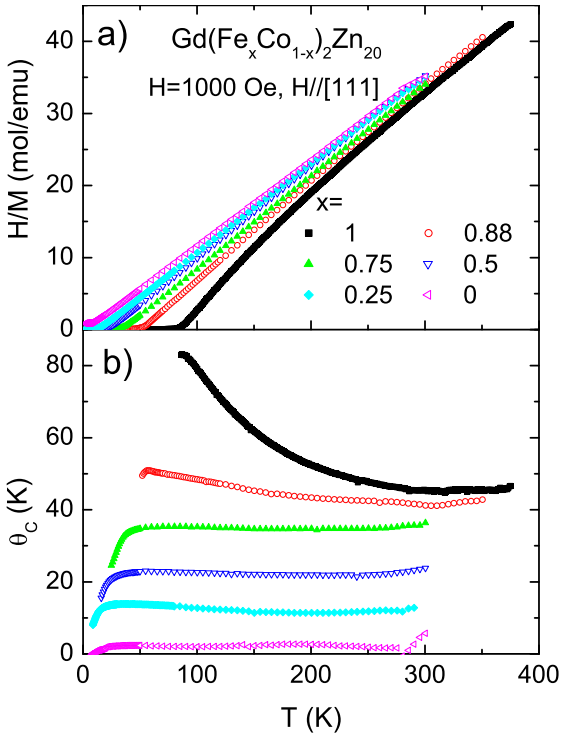

FIG. 27: (color online) (a): H/M ($H = 1000$ kOe) of $Gd(Fe_xCo_{1-x})_2Zn_{20}$ as a function of temperature. (b): temperature varied θ_C. (See text)

composite moment). Assuming an invariant θ_C, values of C can be inferred from:

$$1/C \approx \frac{d(\frac{T-\theta_C}{C})}{dT} = \frac{d(\frac{H}{M})}{dT}. \quad (3)$$

Shown in Fig. 26(c), μ_{eff} manifests a monotonic decrease with decreasing temperature down to 110 K, at which temperature it shows a minimum value 6.6 μ_B. From 100 K to T_C, μ_{eff} starts to rise with a highly non-linear fashion. This rise of the μ_{eff} value is not unexpected in the vicinity of T_C in FM system[42], and could be due to the short range ordering or formation of magnetic clusters of the Gd^{3+} local moment and induced moment. The decrease of μ_{eff}, in this scenario, would be the result of the formation of the magnetic droplets, consisted with the Gd^{+3} local moments and the oppositely polarized electron cloud from the highly polarizable host. Such magnetic droplets are not unprecidented in analogous systems, above T_C. For example, the 'giant moment' was observed in dilute Fe-Pd alloy[43]; the deficient μ_{eff} of local moments was also found in RCo_2 series (R = Gd-Tm)[44] above T_C. Giving that the primary difference between these two alternative explanations is whether

the itinerant electrons are polarized above T_C, Mössbauer spectra measurements on the Fe sites at varied temperature can resolve this paradox.

V. SUMMARY

The six GdT_2Zn_{20} (T = Fe, Ru, Os, Co, Rh and Ir) compounds have magnetic properties that differ dramatically between the Fe column and the Co column members. The Fe column members order ferromagnetically with the enhanced transition temperatures for the T = Fe and Ru members, whereas the Co column members all manifest low-temperature, AFM ordering. In a related manner, the T = Fe and Ru members of YT_2Zn_{20} family manifest typical properties associated with NFFLs. Band structure calculation results for the T = Fe and Ru members reveal that the large DOS at the Fermi level is correlated with the enhancement in the their magnetic properties. The data on the pseudo-ternary series of compounds $Gd(Fe_xCo_{1-x})_2Zn_{20}$ and $Y(Fe_xCo_{1-x})_2Zn_{20}$ further display the effect of the different $3d$-band filling on the magnetic properties of these two series. The conceptually simple framework of the Heisenberg moments embedded in the NFFL, was discussed to understand the enhanced transitions for $GdFe_2Zn_{20}$ and $GdRu_2Zn_{20}$ and the curious temperature dependence of the $1/\chi$ versus T data for $GdFe_2Zn_{20}$.

Acknowledgments

The authors thank J. Frederich for growing some of the compounds, L. Tan for Laue X-ray measurements, E. D. Mun, X. Zong and R. Prozorov for helpful discussions. SLB thanks David Lodge for valuable insights. Ames Laboratory is operated for the U.S. Department of Energy by Iowa State University under Contract No. DE-AC02-07CH11358. This work was supported by the Director for Energy Research, Office of Basic Energy Sciences.

[1] J. J. M. Franse and R. J. Radwanski, in *Handbook of Magnetic Materials* vol. 7 Edited by K.H.J. Buschow (Amsterdam: Elsevier, 1993), pp. 307–501.

[2] A. Szytula and J. Leciejewicz, *Handbook of Crystal Structures and Magnetic Properties of Rare Earth Intermetallics* (CRC Press, 1994).

[3] S. Jia, S. L. Bud'ko, G. D. Samolyuk, and P. C. Canfield, Nat Phys **3**, 334 (2007).

[4] M. S. Torikachvili, S. Jia, E. D. Mun, S. T. Hannahs, R. C. Black, W. K. Neils, D. Martien, S. L. Bud'ko, and P. C. Canfield, PNAS **104**, 9960 (2007).

[5] S. Jia, N. Ni, S. L. Bud'ko, and P. C. Canfield, Physical Review B (Condensed Matter and Materials Physics) **76**, 184410 (2007).

[6] T. Nasch, W. Jeitschko, and U. C. Rodewald, Zeitschrift fuer Naturforschung, B: Chemical Sciences **52**, 1023 (1997).

[7] P. I. Kripyakevich and O. S. Zarechnyuk, Dopov. Akad. Nauk Ukr. RSR, Ser. A **30**, 364 (1968).

[8] V. M. T. Thiede, W. Jeitschko, S. Niemann, and T. Ebel, Journal of Alloys and Compounds **267**, 23 (1998).

[9] O. Moze, L. D. Tung, J. J. M. Franse, and K. H. J. Buschow, Journal of Alloys and Compounds **268**, 39 (1998).

[10] P. C. Canfield and Z. Fisk, Philosophical Magazine Part B **65**, 1117 (1992).

[11] X. Stoe, *AREA-Software Suite for the STOE IPDS II* (Stoe & Cie GmbH, Darmstadt, Germany, 2002).

[12] G. M. Sheldrick and D. SHELXTL, Inc., Madison, WI, USA (2000).

[13] A. Eiling and J. S. Schilling, Journal of Physics F: Metal Physics **11**, 623 (1981).

[14] S. Bud'ko, R. Wilke, M. Angst, and P. Canfield, Physica C: Superconductivity **420**, 83 (2005).

[15] S. Chikazumi and C. Graham, *Physics of Ferromagnetism* (Oxford University Press, 1997).

[16] O. K. Andersen, Phys. Rev. B **12**, 3060 (1975).

[17] O. K. Andersen and O. Jepsen, Phys. Rev. Lett. **53**, 2571 (1984).

[18] U. von Barth and L. Hedin, Journal of Physics C: Solid State Physics **5**, 1629 (1972).

[19] J. P. Perdew, K. Burke, and M. Ernzerhof, Phys. Rev. Lett. **77**, 3865 (1996).

[20] A. Y. Perlov, S. V. Halilov, and H. Eschrig, Phys. Rev. B **61**, 4070 (2000).

[21] G. B. I Turek, J Kudrnovsky and S. Blugel, Journal of Physics: Condensed Matter **15**, 2771 (2003).

[22] From *table of periodic properties of the elements* (Sargent-Welch/VWR Scientific Products, 1998).

[23] A. Arrott, Physical Review **108**, 1394 (1957).

[24] P. E. Brommer and J. J. M. Franse, in *Ferromagnetic Materials* vol 5, edited by K.H.J.

Buschow and E.P. Wohlfarth (Amsterdam: North-Holland, 1990), pp. 323–396.

[25] I. Yeung, R. M. Roshko, and G. Williams, Phys. Rev. B **34**, 3456 (1986).

[26] M. E. Fisher, Philos. Mag. **7**, 1731 (1962).

[27] M. E. Fisher and J. S. Langer, Physical Review Letters **20**, 665 (1968).

[28] J. M. Ziman, *Principles of the Theory of Solids* (Cambridge University Press, 1979).

[29] L. N. Mulay and E. A. Boudreaux, *Theory and applications of molecular diamagnetism* (Wiley, 1976).

[30] χ_0 and γ_0 values of Pd and Pt are extracted from: G. S. Knapp and R. W. Jones, Physical Review B **6**, 1761 (1972); B. Zellermann, A. Paintner and J. Voitländer, J. Phys: Condens. Matter **16**, 919 (2004).

[31] $\gamma_0 = 0.695$ mJ/molK^2 [from C. Kittel, *Introduction to solid state physics* (Wiley New York, 1986)], and $\chi_{0-dia} = 13.4 \times 10^{-6}$ emu/mol (from ref. [29]).

[32] N. W. Ashcroft and N. D. Mermin, *Solid state physics* (Saunders College Philadelphia, Pa, 1976).

[33] M. Shimizu, T. Takahashi, and A. Katsuki, Journal of the Physical Society of Japan **18**, 240 (1963).

[34] S. Tanaka and H. Harima, Journal of the Physical Society of Japan **67**, 2594 (1998).

[35] S. M. Hayden, G. G. Lonzarich, and H. L. Skriver, Phys. Rev. B **33**, 4977 (1986).

[36] M. S. S. Brooks and B. Johansson, in *Handbook of Magnetic Materials* vol. 7 Edited by K.H.J. Buschow (Amsterdam: Elsevier, 1993), pp. 139–230.

[37] I. A. Campbell, Journal of Physics F: Metal Physics **2**, L47 (1972).

[38] G. J. Nieuwenhuys, Advances in Physics **24**, 515 (1975).

[39] J. Crangle, Physical Review Letters **13**, 569 (1964).

[40] N. H. Duc and T. Goto, in *Handbook on the Physics and Chemistry of Rare Earths* vol. 26, edited by K.A. Gschneidner, Jr. and L. Eyring (Amsterdam: Elsevier, 1999), pp. 177–264.

[41] N. H. Duc and P. E. Brommer, in *Handbook of Magnetic Materials,* vol. 12, Edited by K.H.J. Buschow (Amsterdam: Elsevier, 1999), pp. 259–394.

[42] J. A. Mydosh, *Spin Glass: An Experimental Introduction* (Taylor and Francis, London, 1993).

[43] A. M. Clogston, B. T. Matthias, M. Peter, H. J. Williams, E. Corenzwit, and R. C. Sherwood, Physical Review **125**, 541 (1962).

[44] A. M. Stewart, Journal of Physics C: Solid State Physics **17**, 1557 (1984).